Motion and Internal Force Control for Omnidirectional Wheeled Mobile Robots

Dongbin Zhao, Xuyue Deng, and Jianqiang Yi

***Abstract*—This paper presents an integrated scheme for motion control and internal force control for a redundantly actuated omnidirectional wheeled mobile robot. The interactive forces between a robot body and its wheels can be reduced into two orthogonal parts: motion-induced forces and internal forces. First, it is shown that the internal forces reside in the null space of the coefficient matrix of the interactive forces and do not affect robotic motion. However, these forces caused by motor torques should be minimized as much as possible to increase the energy efficiency and life span of joint components. With different goals, the control for motion and the control for internal forces can be designed separately. Here, both kinematic and dynamic models of the forces are proposed. A proportional differential plus controller regulates the motion and an inverse dynamic controller tracks it. Then, to minimize the internal forces, an integral feedback internal force controller is used. The motion controller guarantees the robotic motion while the internal force controller minimizes the internal force occurring during robot motion. Simulation results verify the effectiveness of the proposed schemes.**

***Index Terms*—Internal force control, mobile robots, motion control, redundant systems.**

I. Introduction

An omnidirectional wheeled mobile robot (OWMR) can move in any direction at any time, giving it a remarkable advantage in complicated environments. The problem of the modeling and control of OWMRs is well documented. Bastin et al. [2], [3] addressed the problems in general cases, and Watanabe [15] presented a detailed review of the control approaches up to 1998. Betourne and Campion [1] derived a dynamic model for a class of redundant OWMRs and proposed a feedback control law for trajectory tracking.

Many OWMRs are redundantly actuated making it possible to accomplish additional subtasks such as obstacle avoidance and torque optimization or subjecting the robot to some additional constraints when the basic control goal is achieved. For example, Yi and Kim [18] presented a singularity-free load distribution scheme for an OWMR. For a redundant robot, this is advantageous. But when an OWMR is redundantly actuated, unless the motion of the wheels is very consistent, undesired results, e.g., oscillation, may occur. The consistency of the robot velocity is called the kinematic consistency and that of the acceleration is called the dynamic consistency.

In practice, kinematic consistency is not difficult to attain, whereas dynamic consistency is more complex requiring analysis and control of the interactive forces between the wheels and the robot body. While robot force control has interested researchers for decades [7], [11], [14], this paper also addresses the internal forces since the interactive forces between the robot body and its wheels have been less documented. The interactive forces can be decomposed into two parts: motion-induced forces and internal forces. Only the motion-induced forces contribute to robot motion. The internal forces squeeze or stretch the robot body and its wheels against each other, abrading joint components and reducing their life span. To maximize energy efficiency and the life span of joint components, the internal forces should be minimized. Furthermore, it is possible to control the internal forces independent of the motion-induced forces [5]. In other words, the internal forces can be minimized without affecting robot motion.

This paper proposes an integrated motion and internal force control scheme for redundantly actuated OWMR, motivated by the motion and internal force control in multiple manipulators [12], [13], [16]. The motion-induced forces and internal forces of the OWMR were decomposed orthogonally, and then, a stable motion controller was designed for robot motion regulation and tracking. An internal force controller was designed to minimize the forces produced by motor torque, while robot motion remained unaffected. The internal force control of the special case of a fixed robot orientation was investigated and resolved successfully by Deng *et al.* [4]. This paper presents a general solution for a robot having varied positions and orientations.

This paper is arranged as follows. The kinematics of the OWMR is presented in Section II. The detailed description of the robot motion, the internal force, and torque are given in Section III. The design of the motion and internal force controllers is given in Section IV. Simulations are carried out and the results are presented in Section V. Finally, conclusions are drawn in Section VI.

II. Kinematic Model

The OWMR described here moves on a plane, so its motion can be described in the 2-D global frame *OXY*. The robot is cylindrical with three identical castor wheels fixed symmetrically on the bottom, as shown in Fig. 1(a). Wheels are numbered 1, 2, and 3 and are assigned clockwise with the angle between any two neighboring wheels being $2/3\pi$ with C being the center of the robot body. In the global frame *OXY*, the robot position can be represented by the position of C, which is (x, y). The orientation of the robot is denoted by θ, which is the angle between the axis *OX* and the line crossing C and the center of vertical axis of *wheel* 1. Then, the posture of the robot can be represented by $\xi = (x, y, \theta)^T$.

The top and side views of *wheel i* are shown in Fig. 1(b) and (c), respectively. The radius of each wheel is r. The horizontal distance between C and the center point of the bracket support for each wheel (indicated by F_i) is D. The offset d is the horizontal distance between the center of each wheel O_i and F_i. The angular displacements for wheel rolling and steering are φ_i and η_i, respectively. Assume there is no slippage between *wheel i* and the ground [the velocity constraint is also shown in Fig. 1(c)], then the velocities of O_i and F_i can be derived by

$$\begin{aligned}\vec{V}_{O_i} &= -r\dot{\varphi}_i(\vec{i}\cos\beta_i + \vec{j}\sin\beta_i)\\ \vec{V}_{F_i} &= \vec{V}_{O_i} + \vec{k}\dot{\beta}_i \times \vec{O_iF_i}\\ \vec{V}_{F_i} &= \vec{V}_C + \vec{k}\dot{\theta} \times \vec{CF_i}.\end{aligned} \tag{1}$$

The equations in (1) can be transferred into matrices, which are depicted by

$$\begin{aligned}P_i\dot{\chi}_i &= Q_i\dot{\xi}\\ \dot{\chi}_i &= P_i^{-1}Q_i\dot{\xi} = \bar{J}_i\dot{\xi}\end{aligned} \tag{2}$$

Manuscript received November 7, 2008; revised January 14, 2009 and February 25, 2009. First published April 21, 2009; current version published June 17, 2009. Recommended by Technical Editor G. Yang. This work was supported in part by the National Natural Science Foundation of China (NSFC) Projects 60475030, 60874043, 60575047, and 60621001, in part by the Outstanding Overseas Chinese Scholars Fund of the Chinese Academy of Sciences (2005-1-11), and in part by the Joint Laboratory of Intelligent Sciences and Technology (JL0605).

The authors are with the Key Laboratory of Complex Systems and Intelligence Science, Institute of Automation, Chinese Academy of Sciences, Beijing 100190, China (e-mail: dongbin.zhao@ia.ac.cn; laudon@163.com; jianqiang.yi@ia.ac.cn).

Color versions of one or more of the figures in this paper are available online at http://ieeexplore.ieee.org.

Digital Object Identifier 10.1109/TMECH.2009.2018287

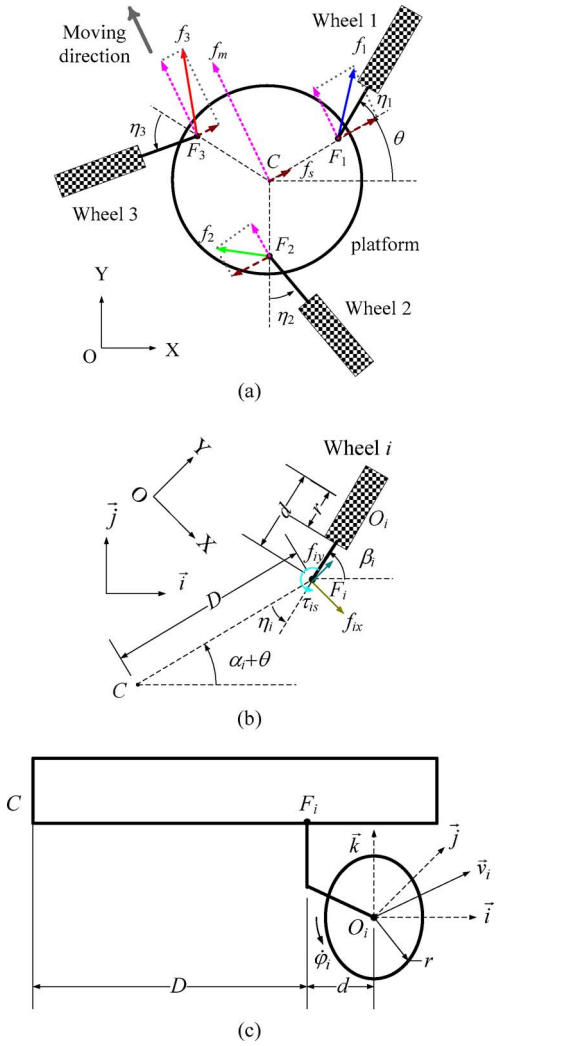

Fig. 1. Wheels assembly of an OWMR with three castors. (a) Whole top view. (b) Top view of *wheel i*. (c) Side view of *wheel i*.

where $\chi_i = (\varphi_i, \eta_i, \theta)^T, i = 1, 2, 3. P_i$ and Q_i are the Jacobian matrices from $\dot{\chi}_i$ and $\dot{\xi}$ to the speed of F_i, respectively, which are denoted by

$$P_i = \begin{bmatrix} -r\cos\beta_i & d\sin\beta_i & d\sin\beta_i \\ -r\sin\beta_i & -d\cos\beta_i & -d\cos\beta_i \\ 0 & 0 & 1 \end{bmatrix}$$

$$Q_i = \begin{bmatrix} 1 & 0 & -D\sin(\alpha_i+\theta) \\ 0 & 1 & D\cos(\alpha_i+\theta) \\ 0 & 0 & 1 \end{bmatrix}$$

$$\bar{J}_i = \begin{bmatrix} -1/r\cos\beta_i & -1/r\sin\beta_i & -D/r\sin\eta_i \\ 1/d\sin\beta_i & -1/d\cos\beta_i & -D/d\cos\eta_i - 1 \\ 0 & 0 & 1 \end{bmatrix}$$

and $\beta_i = \alpha_i + \eta_i + \theta$ is the orientation of *wheel i* in the global frame *OXY*, and $\alpha_1 = 0,\ \alpha_2 = -2/3\pi,$ and $\alpha_3 = 2/3\pi$.

The second row of (2) can be written in a compact matrix form to derive the Jacobian matrix $\bar{J}$ and the transformation from the velocities $\dot{\xi}$ of the robot body to the velocities $\dot{\zeta}$ of its wheels. J can be thought of as its inverse transformation

$$\dot{\zeta} = \bar{J}\dot{\xi} \qquad J\dot{\zeta} = \dot{\xi} \tag{3}$$

where $\zeta = (\varphi_1, \eta_1, \varphi_2, \eta_2, \varphi_3, \eta_3)^T$. $\bar{J}$ can be directly derived from $\bar{J}_i$ by

$$\bar{J} = \begin{bmatrix} -1/r\cos\beta_1 & -1/r\sin\beta_1 & -D/r\sin\eta_1 \\ 1/d\sin\beta_1 & -1/d\cos\beta_1 & -D/d\cos\eta_1 - 1 \\ -1/r\cos\beta_2 & -1/r\sin\beta_2 & -D/r\sin\eta_2 \\ 1/d\sin\beta_2 & -1/d\cos\beta_2 & -D/d\cos\eta_2 - 1 \\ -1/r\cos\beta_3 & -1/r\sin\beta_3 & -D/r\sin\eta_3 \\ 1/d\sin\beta_3 & -1/d\cos\beta_3 & -D/d\cos\eta_3 - 1 \end{bmatrix}.$$

Property 1: If $d/D \leq 1/2$, then rank of $\bar{J}$ is full.

Proof: With 2 or more powered offset castor wheels, $\bar{J}$ is always full rank. A detailed proof can be seen in [4], and a formal one was given in [9].

If Property 1 holds, the matrix J can be achieved by

$$J^T = \bar{J}[\bar{J}^T\bar{J}]^{-1} \tag{4}$$

which will be used in the following motion control design.

III. Dynamic Model

The dynamic model first takes into account the interactive forces acting between the robot body and its wheels. The interactive force is derived and reduced into two orthogonal motion-induced and internal force parts.

A. Dynamic Model With Interactive Forces

Assume the vectors $\tau_i = (\tau_{ir}, \tau_{is})^T$ are the torques produced by the rolling and steering motors of *wheel i*, τ_{di} is the joint torque disturbances caused by the friction of the joint or between the wheel–ground interaction, and f_i is the interactive forces between *wheel i* and the body of the OWMR, which is given by $f_i = (f_{ix}, f_{iy}, \tau_{is})^T$, whose definition is also shown in Fig. 1(b). Since the robot moves in a plane, there is no potential energy, only kinematic energy in K_{χ_i} and K_C. Therefore, K_{χ_i} is the total kinematic energy of *wheel i* and its bracket, and K_C is the kinematic energy at the center of the cylindrical-shaped body of the OWMR. The dynamic model of each wheel in joint space and operational space is derived by

$$\frac{d}{dt}\frac{\partial K_{\chi_i}}{\partial \dot{\chi}_i} - \frac{\partial K_{\chi_i}}{\partial \chi_i} = \begin{bmatrix} \tau_i \\ 0 \end{bmatrix} - \begin{bmatrix} \tau_{di} \\ 0 \end{bmatrix} - P_i^T f_i$$

$$\frac{d}{dt}\frac{\partial K_C}{\partial \dot{\xi}} - \frac{\partial K_C}{\partial \xi} = \sum_{i=1}^{3} Q_i^T f_i. \tag{5}$$

Because φ_i is always orthogonal to η_i, they can be decoupled in K_{χ_i}. Thus, K_{χ_i} and K_C are calculated by

$$K_{\chi_i} = \frac{I_{wb}\dot{\varphi}_i^2}{2} + \frac{I_{bw}\dot{\beta}_i^2}{2}$$

$$K_C = \frac{[m_0(\dot{x}^2 + \dot{y}^2) + I_0\dot{\theta}^2]}{2}$$

where m_0 and I_0 are the mass and inertial moment of the robot body, and I_{wb} and I_{bw} are the inertial moment of the rolling and steering wheels, respectively. Because there are no elements of χ_i or ξ in K_{χ_i} and K_C, the equations $\partial K_C/\partial\xi = 0$ and $\partial K_{\chi_i}/\partial\chi_i = 0$ hold.

Assuming that the wheel units are identical, (5) can be rewritten in a compact matrix form as

$$M_\zeta\ddot{\zeta} = \tau - \tau_d - P^T f$$

$$M_C\ddot{\xi} = Q^T f$$

$$\ddot{\zeta} = \bar{J}\ddot{\xi} + \dot{\bar{J}}\dot{\xi} \tag{6}$$

where f and τ are 9×1 and 6×1 matrices, respectively, and P^T and Q^T are 6×9 and 3×9 "fat" matrices, respectively, which are utilized to describe the relationship of the wheels and the mobile base

$$
\begin{aligned}
f &= [f_1^T, f_2^T, f_3^T]^T \\
\tau &= [\tau_1^T, \tau_2^T, \tau_3^T]^T \\
P^T &= \begin{bmatrix} P_1^T(1:2,:) & & 0 \\ & P_2^T(1:2,:) & \\ 0 & & P_3^T(1:2,:) \end{bmatrix} \\
Q^T &= [Q_1^T, Q_2^T, Q_3^T] \\
M_C &= \mathrm{diag}[m_0, m_0, I_0] \\
M_\zeta &= \mathrm{diag}[I_{wb}, I_{bw}, I_{wb}, I_{bw}, I_{wb}, I_{bw}].
\end{aligned}
$$

The general notion $X(i,:)$ or $X(:,j)$ denotes the ith row or jth column of the matrix X, respectively. The notation diag[*] denotes a diagonal matrix. In control design, the following properties are always assumed to be true.

Property 2: Assume ζ is twice differentiable and $\dot{\zeta}$ and $\ddot{\zeta}$ are bounded.

Property 3: The disturbance torque τ_{di} is bounded.

The third row of the dynamic model (6) is the derivative of (3). By eliminating the acceleration forms, the interactive force f can be derived by

$$f = (M_\zeta \bar{J} M_C^{-1} Q^T + P^T)^{-1}(\tau - \tau_d - M_\zeta \dot{\bar{J}}\dot{\xi}) \tag{7}$$

where the matrix $(M_\zeta \bar{J} M_C^{-1} Q^T + P^T)(M_\zeta \bar{J} M_C^{-1} Q^T + P^T)^T$ is nonsingular, so the inverse matrix of the $M_\zeta \bar{J} M_C^{-1} Q^T + P^T$ can be derived by the left Moore–Penrose method.

B. Interactive Forces to Internal Forces

The matrix Q^T is a 3×9 "fat" matrix with full row rank, which possesses a nontrivial null space. If there is a 9×1 vector υ lying in the kernel of the null space of Q^T, $Q^T \upsilon = 0$ always holds. The second equation of (6) indicates that if the right-hand side equals zero, then the acceleration term on the left-hand side should also be zero, and the robot motion is not affected by υ. That is to say, one part of the interactive force f residing in the kernel of the null space of Q^T does not affect robot motion.

The kernel of the null space of Q^T is defined as $X_s = \mathrm{Ker}(Q^T)$, which defines the internal force subspace. The image or range space of Q^T is defined as $X_m = \mathrm{Im}(Q^T)$, which is the motion subspace orthogonal to X_s. The interactive force f can be uniquely decomposed into two orthogonal parts: the motion-induced force f_m and the internal force f_s, subject to the motion and internal subspaces, respectively,

$$f = f_m + f_s \tag{8}$$

where $f_m \in X_m$ and $f_s \in X_s$. So, only f_m contributes to the motion of the mobile robot. As shown in Fig. 1(a), f_m is in the same direction as the robot motion and f_s is orthogonal to the motion direction. The internal force f_s is calculated by projecting the interactive force f on the internal force subspace X_s.

However, Q^T is a function of the orientation angle θ, not a constant matrix, so it is difficult to calculate the kernel and range space of Q^T. A mathematical transform is applied by

$$Q^T = Q_c^T \hat{Q}^T \tag{9}$$

where $Q_c^T = [1_3, 1_3, 1_3]$ and $\hat{Q}^T$ is invertible

$$\hat{Q}^T = \begin{bmatrix} Q_1^T & & 0 \\ & Q_2^T & \\ 0 & & Q_3^T \end{bmatrix}.$$

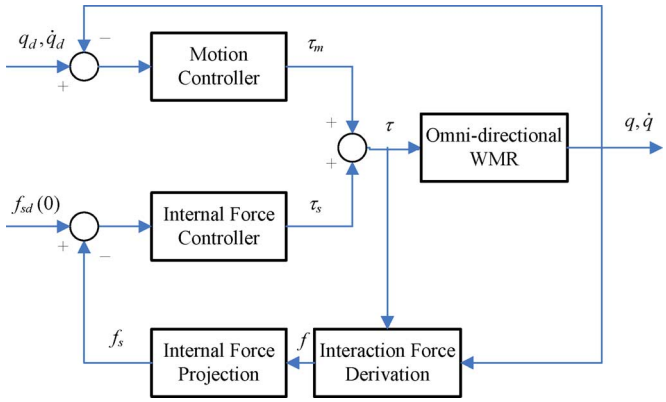

Fig. 2. Motion and internal force control scheme of the OWMR.

As opposed to Q^T, Q_c^T is a constant matrix, which does not have the problem of unit consistency. Thus, Q_c^T is applied instead of Q^T to calculate the motion and internal force subspaces. A pair of orthogonal projections on each subspace is defined by

$$
\begin{aligned}
Pr_m &= Q_c(Q_c^T Q_c)^{-1} Q_c^T \\
Pr_s &= 1_9 - Q_c(Q_c^T Q_c)^{-1} Q_c^T.
\end{aligned} \tag{10}
$$

Then, by left-multiplying $\hat{Q}^T$, (8) can be rewritten as

$$f_c = f_{cm} + f_{cs} \tag{11}$$

where $f_c = \hat{Q}^T f$ is the corrected interactive force. $f_{cm} = \hat{Q}^T f_m$ and $f_{cs} = \hat{Q}^T f_s$ are the corrected motion-induced force and internal force, which are used for calculation and controller design. f_{cm} and f_{cs} are projected into the aforementioned subspaces and derived by $f_{cm} = Pr_m f_c \in \mathrm{Im}(Q_c^T)$ and $f_{cs} = Pr_s f_c \in \mathrm{Ker}(Q_c^T)$, respectively.

IV. Motion and Internal Force Control

From the dynamic model (6), motor torque is derived as $\tau = P^T f$, which can also be decomposed into two parts. As indicated in [16], the internal force does not affect the robot motion, but robot motion will affect the internal force due to the internal component of the inertial force. This suggests the control scheme as

$$
\begin{aligned}
\tau &= \tau_m + \tau_s \\
\tau_s &= P^T f_s
\end{aligned} \tag{12}
$$

where τ_m controls motion torque and τ_s regulates the internal force. These controls can be designed separately, and then integrated. Generally, the proposed motion and internal force controls are depicted as follows: first, a stable motion controller τ_m is designed; then, an internal force controller τ_s is constructed to reduce the internal force f_s to zero. The integrated control scheme is shown in Fig. 2.

A. Regulation Control

The motion controller is designed to regulate the posture of the robot to ξ_r, a constant vector. A proportional differential plus controller is designed by

$$\tau_m = -J^T(K_p \xi_e + K_d \dot{\xi}) - G\dot{\zeta} \tag{13}$$

where K_p, K_d, and G are diagonal positive matrices with proper dimensions, and $\xi_e = \xi - \xi_r$.

Proposition 1: The motion controller stabilizes the robot.

Proof: $\forall t < \infty$, $\int_0^t \dot{\zeta}^T(s)\tau_d(s)ds$ is bounded according to Properties 2 and 3. The Lyapunov function is defined as

$$V = \frac{\dot{\xi}^T M_C \dot{\xi}}{2} + \frac{\dot{\chi}^T M_\chi \dot{\chi}}{2} + \frac{\xi_e^T K_p \xi_e}{2} + \int_0^t \dot{\zeta}^T(s)\tau_d(s)ds + K_0 \quad (14)$$

where K_0 can be chosen to be positive and large enough to ensure that $\int_0^t \dot{\zeta}^T(s)\tau_d(s)ds + K_0 > 0$ and $V > 0$. The derivative of the Lyapunov function is calculated by

$$\begin{aligned}\dot{V} &= \dot{\xi}^T M_C \ddot{\xi} + \dot{\chi}^T M_\chi \ddot{\chi} + \dot{\xi}^T K_p \xi_e + \dot{\zeta}^T \tau_d \\ &= \dot{\xi}^T [\bar{J}^T(\tau_m - \tau_d) + K_p \xi_e] + \dot{\zeta}^T \tau_d \\ &= -\dot{\xi}^T K_d \dot{\xi} - \dot{\zeta}^T G \dot{\zeta} \le 0.\end{aligned}$$

B. Tracking Control

An inverse dynamic controller is designed for tracking control. The dynamic model (6) can be rewritten without consideration of the interactive force as

$$M_\zeta \ddot{\zeta} = \tau - \tau_d. \quad (15)$$

By left-multiplying $\bar{J}^T$ to both sides of (15), one can obtain

$$\bar{J}^T M_\zeta \ddot{\zeta} = \bar{J}^T(\tau - \tau_d). \quad (16)$$

Thus, the tracking controller is designed with

$$\begin{aligned}\tau_m &= M_\zeta \ddot{\zeta}_0 \\ \ddot{\zeta}_0 &= \bar{J}\left(\ddot{\xi}_r - K_d\dot{\xi}_e - K_p\xi_e - K_i\int_0^t \xi_e(s)ds\right) + \dot{\bar{J}}\dot{\xi}\end{aligned} \quad (17)$$

where K_p, K_d, and K_i are diagonal positive matrices with proper dimensions. Substituting (17) into (16) results in

$$\bar{J}^T M_\zeta \bar{J}\left(\ddot{\xi}_e + K_d\dot{\xi}_e + K_p\xi_e + K_i\int_0^t \xi_e(s)ds\right) + \bar{J}^T\tau_d = 0 \quad (18)$$

where $\bar{J}^T M_\zeta \bar{J}$ is not a singular matrix. Therefore, (18) implies that when $t \to \infty, \xi_e$ converges to zero if $\tau_d = 0$.

C. Internal Force Control

An integral feedback internal force is applied by

$$\begin{aligned}\tau_s &= P_C^T \hat{Q}^{-T} F_{cs} \\ F_{cs} &= f_{cs_{\text{des}}} - \Omega\int_0^t \left(f_{cs}(s) - f_{cs_{\text{des}}}\right)ds, f_{cs_{\text{des}}} \in \text{Ker}(Q_C^T)\end{aligned} \quad (19)$$

where Ω is a 9×9 diagonal matrix. Unlike the case of multiple manipulators, the desired internal force $f_{cs_{des}}$ residing in the kernel of the null space should be zero for the OWMR.

Though the integral term may cause F_{cs} to exceed the boundaries of the linear space of Ker(Q_C^T), a unique equilibrium, may not be the original one, can eventually be achieved [8].

V. Simulation

The robot shown in Fig. 1(a) is simulated to verify the proposed motion and internal force control scheme. Table I gives the parametric values of the dynamic models. The data are measured in SI standard units, but are omitted in the table and discussion for clarity.

TABLE I
Parameters Values of the Dynamic Models

r	d	D	m_0	I_0	I_{wb}	I_{bw}
0.1	0.015	0.2	60	0.3	0.15	0.05

A. Regulation With Proportional Derivative Control

In the simulations, performance comparisons are carried out for torque control with and without the internal force feedback controller.

The disturbance torque τ_d is introduced to verify the robustness of the proposed controller, and assumed to be a dead zone for motor torque output

$$\tau_{dk} = -\text{sign}(\tau_k)\tau_{Lk}, \qquad k = 1, 2, \ldots, 6 \quad (20)$$

where τ_L is the upper bound of the motor torque output dead zone, which is given by $\tau_L = (0.02, 0.01, 0.02, 0.01, 0.02, 0.01)^T$.

The robot's initial posture states are set $\xi_0 = (5, 4, \pi)^T$, and its initial wheel states are set $\zeta_0 = (0, 1, 0, 2, 0, 3)^T$. The destination posture states are set $\xi_r = (0, 0, 0)^T$.

The motion regulation controller and internal force controller are adopted and combined (Fig. 2) using the control parameters

$$\begin{aligned}K_p &= \text{diag}[2.5, 2.5, 2.5] \\ K_d &= \text{diag}[0.5, 0.5, 0.5] \\ G &= \text{diag}[0.5, 0.5, 0.5] \\ \Omega &= \text{diag}[10, 10, 2, 10, 10, 2, 10, 10, 2].\end{aligned}$$

In Fig. 3(a)–(c), dashed-dotted and solid lines represent the motion regulation simulation results without and with the internal force feedback controller, respectively.

The linear speed $v = \sqrt{\dot{x}^2 + \dot{y}^2}$ of the robot is shown in Fig. 3(a), and the orientation speed is shown in Fig. 3(b). As expected, the internal force controller does not affect the stability of the motion controller. But the internal force controller reduces the overshot of speed response, and a better transient performance is obtained.

For performance comparison, an index associated with the output torque is defined

$$\bar{\tau} = \tau^T \tau \quad (21)$$

where $\bar{\tau}$ can be regarded as a scale of consumed energies. Fig. 3(c) shows that the internal force controller reduces the energy consumption making it ideal for implementation in real systems.

Fig. 3(d) and (e) shows the internal force along the X-axis of the global frame without and with the internal force controller. In each figure, the dash-dotted line, the dashed line, and the solid line denote the internal force profile at the contact point F_1, F_2, and F_3 [see Fig. 1(a)], respectively. The amplitudes of the internal forces without the control are much larger than that with it. The internal force in both cases converges, but when the internal force control is implemented, it zeros in a shorter time.

B. Tracking With Inverse Dynamic Control

The robot's initial posture is $\xi_0 = (2, 2, 0)^T$, and its initial wheel states are $\zeta_0 = (0, 1, 0, 2, 0, 3)^T$, which is the same as in the regulation case. The robot is required to follow the trajectory

$$\begin{cases}x(t) = 4 + 4\sin t/40 \\ y(t) = 3 + 3\sin t/20 \\ \theta(t) = \pi + \pi\sin t/40.\end{cases} \quad (22)$$

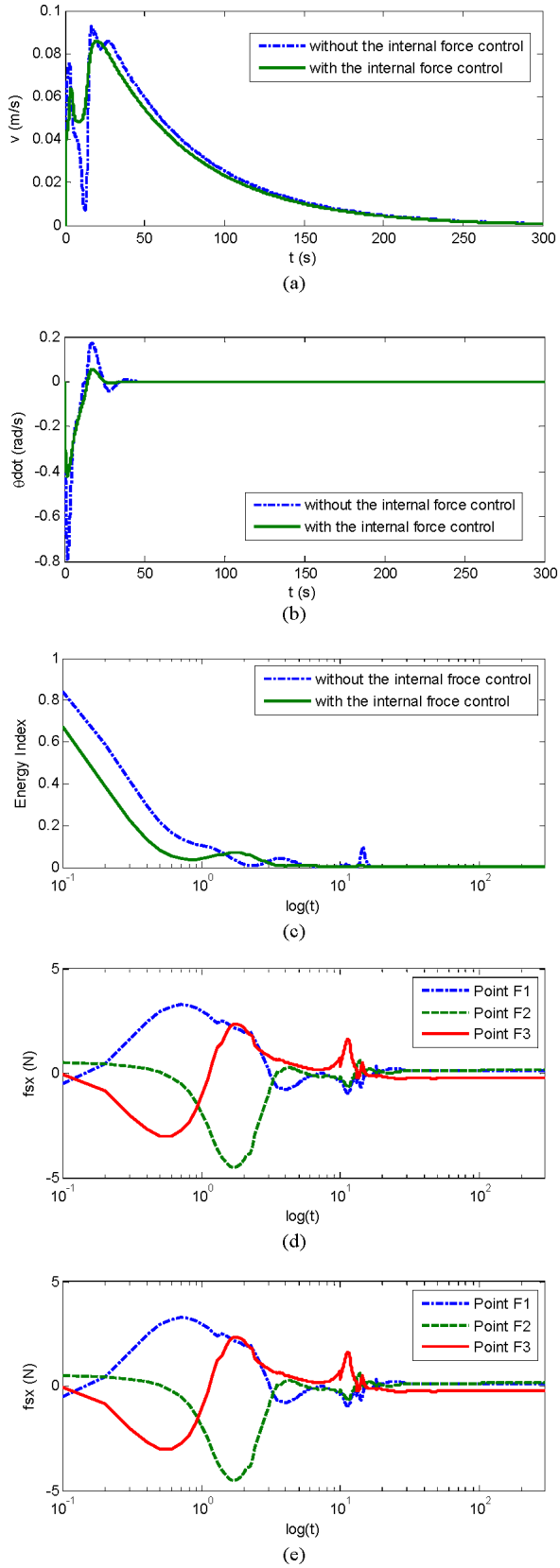

Fig. 3. Regulation with proportional derivative ç control. (a) Linear speed response comparison. (b) Orientation speed response comparison. (c) Energy cost comparison. (d) Internal forces along X-axis without the internal force control. (e) Internal forces along X-axis with the internal force control.

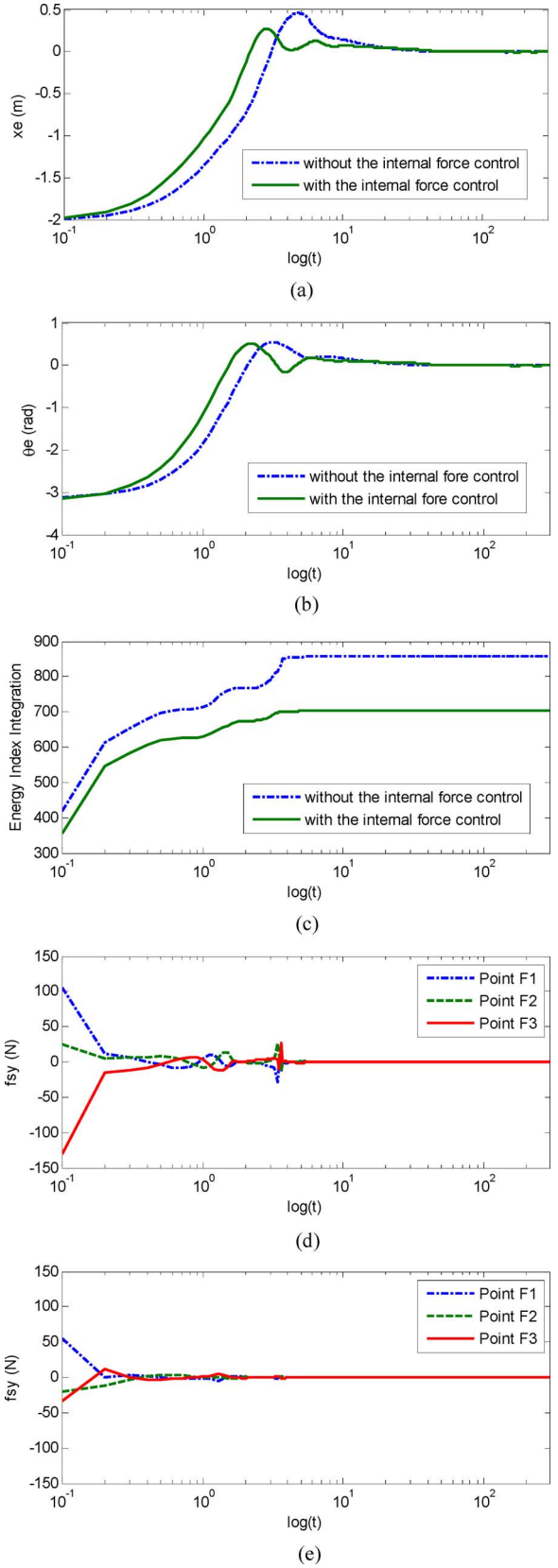

Fig. 4. Tracking with inverse dynamic control. (a) Position errors comparison along X-axis. (b) Orientation errors comparison. (c) Energy cost integration comparison. (d) Internal forces along Y-axis without the internal force control. (e) Internal forces along Y-axis with the internal force control.

The motion tracking and internal force controller are applied, and the control parameters are

$$K_p = \text{diag}[5, 5, 5]$$
$$K_d = \text{diag}[2.5, 2.5, 2.5]$$
$$K_i = \text{diag}[0.25, 0.25, 0.25]$$
$$\Omega = \text{diag}[25, 25, 10, 25, 25, 10, 25, 25, 10].$$

The position and orientation errors of the tracking control are shown in Fig. 4(a) and (b). The results show that the trajectory of the robot is successfully tracked with the motion controller. Computational errors and the influence of the disturbance torque τ_d on the internal force controller may affect robot motion to some extent. But the stability of the robot motion is not affected and tracking errors are limited. The tracking errors along the X-axis (similar to those along the Y-axis) and orientation are similar with and without the internal force control, but the transient response with the controller improves performance.

To be more succinct, the integration of the torque index, defined as (21) in the regulation case, is calculated and shown in Fig. 4(c). The consumed energy is effectively reduced when using the internal force controller.

The internal forces along the Y-axis (similar to those along the X-axis) without and with the internal force control are shown in Fig. 4(d) and (e), respectively. The internal forces are reduced significantly benefiting energy efficiency and the life span of the wheel units. For the posture tracking problem, unlike the regulation case, the internal force could not be reduced to zero, although they fluctuate around zero. Repeated experiments indicate that the gain in control should be larger in the case of tracking control than in regulation to guarantee that the internal force is reduced effectively.

VI. Conclusion and Future Work

The major contribution of this paper is the derivation of the kinematic and dynamic models of the interactive forces of the OWMR specifically between the robot body and its wheels, and the presentation of an integrated control scheme for the robot motion and internal forces.

Interactive forces are decomposed into two orthogonal parts: motion-induced forces and internal forces. In theory, if internal forces reside strictly in the null space of the coefficient matrix of the interactive forces, neither robot motion nor localization accuracy will be affected. This conclusion is verified by motion regulation and tracking simulation results, which are similar to those in multiple manipulator cases.

In robot motion control, motion controllers are designed with a proportional differential plus controller for regulation and an inverse dynamic controller for tracking. At the same time, internal forces caused by robot motion are reduced by an integral feedback internal force controller. With the proposed control scheme, the stability of robot motion is guaranteed and internal forces are efficiently reduced to increase the energy efficiency of the system and the life span of joint components. For the disturbances or unidentified uncertainties, effective robust control schemes should be utilized, which are referred to in our work [17]. Moreover, unlike multiple manipulator cases with fixed bases, the motion of OWMRs is based on movable wheels. Therefore, internal forces may coact with motion-induced forces on the wheels to cause their slippage [6], [10]. This is another interesting problem for future research.

The motion and internal force control strategy is proposed for an OWMR with three castor wheels. It is derived from each independent wheel to achieve a generalized form, which can be easily extended to other typical OWMR systems with four or six castor wheels.

Acknowledgment

The authors would like to thank Prof. J. T. Wen of Rensselaer Polytechnic Institute and the anonymous reviewers for their constructive suggestions on this research, and R. Capen and C. Capen for help with a draft of the paper.

References

[1] A. Betourne and G. Campion, "Dynamic model and control design of a class of omnidirectional mobile robots," in *Proc. 1996 IEEE Int. Conf. Robot. Autom.*, pp. 2810–2815.
[2] G. Campion, G. Bastin, and B. D. Andrea-Novel, "Structural properties and classification of kinematic and dynamic models of wheeled mobile robots," *IEEE Trans. Robot. Autom.*, vol. 12, no. 1, pp. 47–62, Feb. 1996.
[3] C. C. de Wit, B. Siciliano, and G. Bastin, Eds., *Theory of Robot Control*. New York: Springer-Verlag, 1996.
[4] X. Y. Deng, D. B. Zhao, J. Q. Yi, and J. T. Wen, "Motion and squeeze force control for omnidirectional wheeled mobile robots," in *Proc. Amer. Control Conf.*, 2006, pp. 5608–5613.
[5] C. S. Kim, S. S. Park, and C. K. Park, "Robust position, motion-induced force, and internal force control for multi-robot system," in *Proc. 6th IEEE Int. Workshop Robot Human Commun.*, 1997, pp. 82–87.
[6] C. B. Low and D. W. Wang, "GPS-based tracking control for a car-like wheeled mobile robot with skidding and slipping," *IEEE/ASME Trans. Mechatronics*, vol. 13, no. 4, pp. 480–484, Aug. 2008.
[7] J. K. Mills, "Robotic manipulator control of generalized contact force and position," *IEEE Trans. Syst., Man, Cybern.*, vol. 24, no. 3, pp. 523–531, Mar. 1994.
[8] G. Montemayor and J. T. Wen, "Decentralized collaborative load transport by multiple robots," in *Proc. 2005 IEEE Int. Conf. Robot. Autom.*, pp. 374–379.
[9] D. Oetomo and M. H. Ang, Jr, "Singularity-free joint actuation strategy for omnidirectional mobile platforms with powered offset caster wheels," *ASME J. Mech. Des.*, vol. 130, no. 5, pp. 054501.1–054501.5, May 2008.
[10] G. Reina, L. Ojeda, A. Milella, and J. Borenstein, "Wheel slippage and sinkage detection for planetary rovers," *IEEE/ASME Trans. Mechatronics*, vol. 11, no. 2, pp. 185–195, Apr. 2006.
[11] B. Siciliano and L. Villani, *Robot Force Control*. Norwell, MA: Kluwer, 1999.
[12] D. Sun and J. K. Mills, "Manipulating rigid payloads with multiple robots using compliant grippers," *IEEE/ASME Trans. Mechatronics*, vol. 7, no. 1, pp. 23–34, Mar. 2002.
[13] I. D. Walker, S. I. Marcus, and R. A. Freeman, "Distribution of dynamic loads for multiple cooperating robot manipulators," *J. Robot. Syst.*, vol. 6, no. 1, pp. 35–47, 1989.
[14] Z. P. Wang, S. S. Ge, and T. H. Lee, "Robust motion/force control of uncertain holonomic/nonholonomic mechanical systems," *IEEE/ASME Trans. Mechatronics*, vol. 9, no. 1, pp. 118–123, Mar. 2004.
[15] K. Watanabe, "Control of an omnidirectional mobile robot," in *Proc. Int. Conf. Knowl.-Based Intell. Electron. Syst.*, 1998, pp. 51–60.
[16] J. T. Wen and K. Kreutz-Delgado, "Motion and force control of multiple robotic manipulators," *Automatica*, vol. 28, no. 4, pp. 729–743, 1992.
[17] D. Xu, D. B. Zhao, J. Q. Yi, and X. M. Tan, "Trajectory tracking control of omnidirectional wheeled mobile manipulators: Robust neural network based sliding mode approach," *IEEE Trans. Syst., Man, Cybern. B, Cybern.*, vol. 39, no. 3, pp. 788–799, 2009.
[18] B. J. Yi and W. K. Kim, "The kinematics for redundantly actuated omnidirectional mobile robots," in *Proc. IEEE Int. Conf. Robot. Autom.*, 2000, pp. 2485–2492.